Journal Name

Dynamic Article Links ►

Cite this: DOI: 10.1039/c0xx00000x

www.rsc.org/xxxxxx

ARTICLE TYPE

Photolytic water oxidation catalyzed by a molecular carbene iridium complex

Ana Petronilho,[a,b] Mahfujur Rahman,[b,c] James A. Woods,[d] Haris Al-Sayyed,[a] Helge Müller-Bunz,[a] J. M. Don MacElroy,[b,c] Stefan Bernhard[d] and Martin Albrecht*[a,b]

Received (in XXX, XXX) Xth XXXXXXXXX 20XX, Accepted Xth XXXXXXXXX 20XX

DOI: 10.1039/b000000x

The complex $IrCl_2(Cp^*)(trz)$ (trz = triazolylidene), **2**, was prepared from readily available 1,3-dimethyl-4-phenyl-1,2,3-triazolium salt. Under basic conditions, the C-bound phenyl group readily cyclometalates, while under acidic conditions, cyclometalation is reversed. The sensitivity of the C_{aryl}–Ir bond but not the C_{trz}–Ir bond towards acidolysis provided a basis for using **2** as catalyst in Ce^{IV}-mediated water oxidation. The catalytic activity is characterized by a robust catalytic cycle, affording excellent turnover numbers (TON > 20,000). Under cerium-free conditions and in the presence of hematite as photoelectrode, light-induced activity was observed. The photoelectrochemical reaction is strongly pH-dependent which requires pH adjustments when running multiple cycle experiments to regenerate the catalytic activity. Analogous chelating complexes display better stability and higher catalytic activity than the monodentate complex **2**.

Introduction

The pursuit of sustainable energy sources has gained increasing importance in the last years due to concerns related to global warming and growing demands in energy supplies. One obvious target is the use of energy from the sun, since it provides 1.2×10^5 TW of radiation to the surface of the Earth, far in excess of global energy needs.[1] Recent efforts to harness this transient energy concentrated on the storage of solar energy into chemical bonding energy. This concept is strongly inspired by biological systems such as photosystem II,[2] which effectively utilizes light to split water into O_2 and H^+ ions that power ATP synthase to replenish biological energy reservoirs. While natural photosynthesis is fast and efficient, the complex sequence of cascade reactions involved in photosynthetic water splitting requires artificial mimicry to render the process technologically exploitable.[3]

Because of the challenges of the water oxidation half cycle in a putative water splitting process,[4] largely due to the high uphill thermodynamic barrier and the complexity involved in the microscopic steps of the O–O bond forming process,[5] recent work on artificial photosynthesis targeted predominantly the development of efficient catalysts for water oxidation.[6] Inspired by the Mn_4Ca cluster of the oxygen-evolving complex (OEC) in photosystem II, significant progress has been accomplished by using di- and tetrametallic complexes,[7] in which metal-metal cooperativity lowers the redox demand of each metal center. More recently, single site catalysts emerged as a powerful class of catalyst precursors,[8] most of which are comprised of a ligand that is non-innocent and that assists the oxidation process through concomitant proton transfer (proton-coupled electron transfer, PCET).[9] Specifically, IrCp*-containing systems afforded a class of catalyst precursors that showed excellent performance in water oxidation mediated by a sacrificial oxidant, typically cerium ammonium nitrate (CAN),[10] although the mode of action of these IrCp* complexes (Cp* = pentamethylcyclopentadienyl, $C_5Me_5^-$) has been discussed controversially.[11,12] A heterogenization has been put forward in parts because of similar performance of these complexes, $IrCl_3$, and iridium nanoparticles, and also because of complex degradation observed after water oxidation.[11] Kinetic and quartz microbalance measurements on specific complexes support, however, homogeneous water oxidation.[11a,12] Our investigations using chelating triazolylidene IrCp* complexes[12] (where triazolylidene is the mesoionic carbene derived from a 1,2,3-triazolium salt)[13] have been concurring thus far with homogeneous water oxidation. The high activity of these complexes has been rationalized in parts by the mesoionic character of the ligand and its tendency to transiently absorb a proton,[14] thus providing access to a PCET process. These triazolylidene iridium complexes are highly robust in the presence of CAN as sacrificial oxidant (TONs > 40,000), which suggests this type of complex as promising active site for sustainable applications. We were therefore interested to probe whether photoelectrochemical methods are feasible to substitute CAN as sacrificial oxidant.[3f,15] To this end, we report here on the CAN-mediated and the photoelectrode-assisted catalytic activity of a simple triazolylidene iridium complex in water oxidation. We have evaluated various set-ups using α-Fe_2O_3 as photoabsorber[16] and focused in particular on the relevance of the pH and on the effect of NaCl on the water oxidation capacity. Appropriate engineering of the conditions provided a system that remains photoelectrochemically active after >20 cycles.

Results and discussion

Synthesis of the complexes

Complex **2** featuring a monodentate bonding mesoionic triazolylidene represents a simpler congener of the chelating complexes reported earlier.[10b] This complex is readily available from the corresponding triazolium salt **1** via Ag_2O-mediated proton abstraction and in-situ metallation with $[Ir(Cp^*)Cl_2]_2$ in a one-pot procedure (Scheme 1). Complex **2** is air-stable both in the solid state and in solution over extended periods of time (> months). It is well soluble in chlorinated solvents and MeCN, though only sparingly soluble in H_2O. Ultrasonication increases the solubility in aqueous media. In the NMR spectrum ($CDCl_3$ solution), **2** is characterized by a symmetric phenyl group, suggesting fast rotation about the C_{trz}–C_{Ph} bond. The iridium-bound carbene appears at δ_C 144.9 ppm.

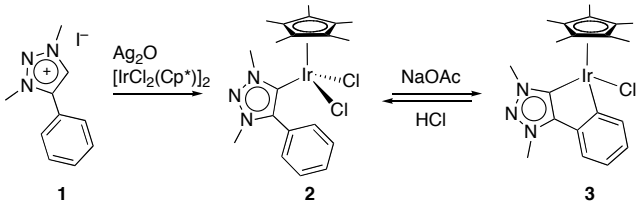

Scheme 1 Synthesis of complexes **2** and its reversible cyclometalation.

Unambigous confirmation of the structure of complex **2** was obtained by X-ray diffraction analysis of single crystals. The molecular structure (Fig. 1) displays the expected piano-stool arrangement. The unsupported Ir–C11 bond in **2** is significantly longer than the analogous bond in chelating species (2.052(1) Å *vs* 2.00–2.02 Å).[10b] As observed in other triazolylidene metal complexes,[13a,17] the heterocyclic C=C bond is considerably stretched upon metal coordination. In complex **2**, this bond is 1.408(2) Å (*cf.* 1.36 Å in triazolium salts similar to **1**).[13b,18] The heterocyclic and the phenyl ring planes are mutually twisted by about 60°.

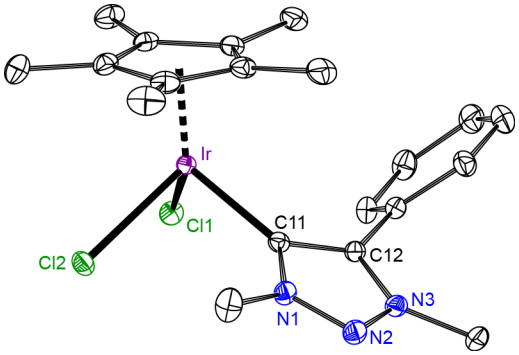

Fig. 1 ORTEP plot of complex **2** (50% probability, hydrogen atoms and co-crystallized CH_2Cl_2 molecule omitted for clarity). Selected bond lengths (Å) and angles (°): Ir–C11 2.0521(14), Ir–Cl1 2.4164(3), Ir–Cl2 2.4335(3), Ir–Cp(centroid) 1.801(1), C11–Ir–Cl1 92.97(4), C11–Ir–Cl2 93.86(4), Cl1–Ir–Cl2 84.471(12).

When treated with a base (NaOAc), cyclometalation and formation of complex **3** is induced. At room temperature, this process is slow and requires several days to go to completion. At higher temperatures, cyclometalation is considerably accelerated (12 h at 60 °C in $C_2H_4Cl_2$). Formation of the iridacycle is most diagnostically identified by the desymmetrization of the aryl substituents and by the loss of one proton in the integral. Whereas in **2**, the phenyl protons appear as two multiplets, four distinct resonance patterns are observed for complex **3** comprised of two doublets and two triplets. In addition, one of the N-bound methyl groups shifts from δ_H 3.7 in **2** to δ_H 4.2 in **3**, presumably as a direct consequence of the coplanar arrangement of the heterocycle and the aryl group in **3**. In the ^{13}C NMR spectrum, the carbene resonance is shifted about 10 ppm to lower field and appears at 154 ppm.

In the presence of acid (HCl, 1 M), the cyclometalation is reverted and complex **2** is cleanly regenerated.[19] Acidolysis in the presence of DCl in D_2O afforded the monodeuterated species **2–D_1** exclusively, implying that the C–Ir bond cleavage is irreversible at pH 1. Under these conditions, no traces of triazolium salt **1** was observed. Hence, the C_{aryl}–Ir bond is substantially less stable than the C_{trz}–Ir bond. Despite the lack of support through chelation, the C_{trz}–Ir bond resists cleavage. This stability is particularly relevant for application of complex **2** under acidic conditions (see below). The lability of complex **2** towards pH (and presumably oxidation-state) dependent cyclometalation is of potential interest for redox catalysis, as transient formation of a metallacycle akin to **3** may provide a powerful proton acceptor site and thus assist metal-centered oxidation processes, enabling proton-coupled electron transfer.[9]

Ce^{IV}-mediated water oxidation

Complex **2** was evaluated in water oxidation catalysis in the presence of sacrificial cerium ammonium nitrate (CAN). Due to substantially lower solubility of **2** in water, measurements were

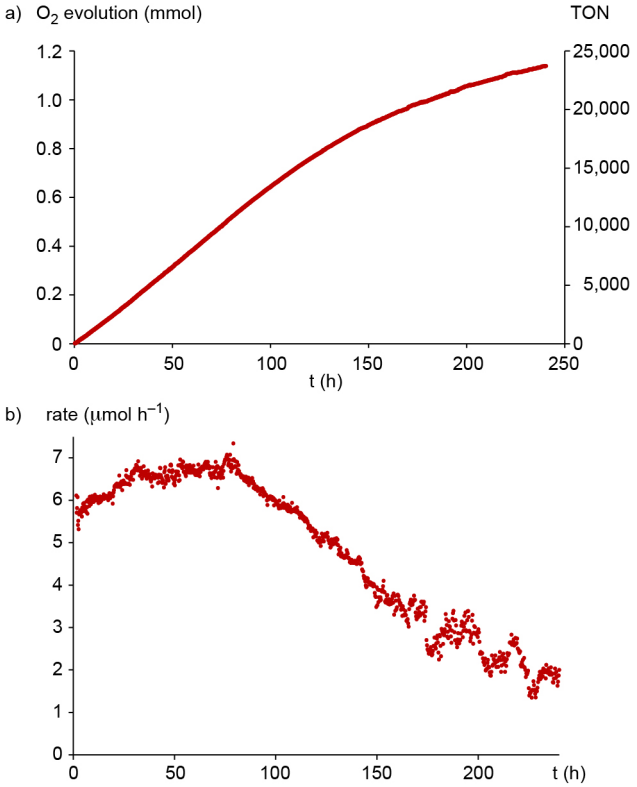

Fig. 2 a) O_2 evolution (measured by manometry and calibrated by GC and TONs over 250 h using complex **2** (50 nmol) and mmol CAN (10 mmol) in water (10 mL); b) time-dependence of observed O_2 evolution rate.

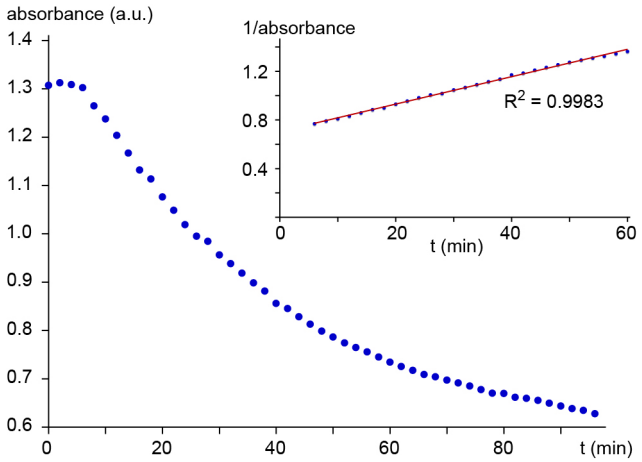

Fig. 3 Time-dependent absorbance at 580 nm (1.4 mM catalyst, 20 molequiv CAN in 2.0 mL H_2O); inset shows the correlation of the inverse absorbance *vs* time (blue dots) and the linear fit (red line), indicating second order kinetics.

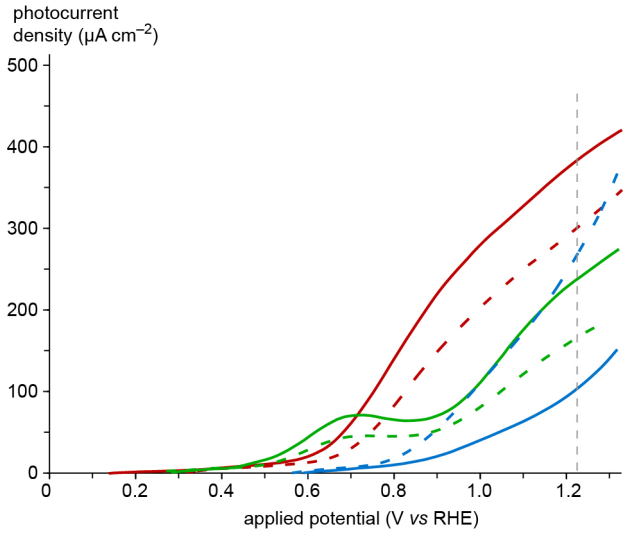

Fig. 4 Photocurrent generated in the presence of complex **2** (27 μM) and hematite (solid lines) and by hematite only (dashed lines, un-catalyzed background) at different pH (blue: pH 13.6, green: pH 7; red: pH 3.3; 3.5% NaCl used as electrolyte).

performed at low complex concentration (ratio **2**/CAN ca. 1:200,000). Under these conditions, O_2 evolution was observed to be almost constant for about a week (Fig. 2a). Longer reaction times led to a gradual decrease of O_2 evolution, reaching a total TON of 22,800 after 10 days (with respect to CAN). Detailed analysis of the O_2 evolution rate indicates that O_2 production is essentially constant over the first 60 h (Fig. 2b). The initial turnover frequency (120 h^{-1}) is substantially lower when compared with the activity of chelating species, indicating a beneficial role of the chelate on the catalytic performance.[10b] After 60 h, the O_2 evolution rate gradually decreases. After 10 days, only approximately 25% of the initial rate was observed, despite the availability of plentiful CAN (ca. 50% not consumed at this stage). This loss of activity points to a limited longevity of the catalytically active species,[20] which contrasts the long-term activity observed for iridium complexes with chelating triazolylidene ligands.[10b,12] Nonetheless, the productivity of complex **2** is remarkable and is one of the highest reported thus far for non-electrochemical O_2 evolution.

When water oxidation was carried with a small excess CAN only (10-100 molequiv.), a blue color appeared. While this color has often been associated with the formation of nanoparticles,[11] it is worth noting that in catalytic runs using **2**, the blue color is not persistent and gradually disappears (Fig. 3, S2). The disappearance occurs over two stages, though only the first process is correlated with O_2 evolution.[12] The time required to re-establish the original yellow color of the solution depends on the number of equivalents of CAN added. With 10 molequiv, it took approximately 2 h, while addition of 80 molequiv resulted in a longer persistence of the blue color (ca. 2 d, Fig. S1). The first decay of the absorption of this blue intermediate (at λ_{max} = 580 nm) is second order, as the plot of the inverse absorbance *vs* time is linear (inset Fig. 3). Although heterogeneous water oxidation cannot be confidently discarded, these data support the presence of a molecular catalyst as active species, and the observed second order transformation likely involves two iridium centers. This hypothesis agrees well with preceding studies, which concluded that the rate-limiting step in molecular water oxidation is associated either with O–O bond formation, *e.g.* via interaction of two metal–oxo species, or with the generation of a springloaded M=O species, *e.g.* via disproportionation.[5]

Photoelectrochemical activity

A photoelectrochemical cell was used in an attempt to substitute the sacrificial oxidant CAN ultimately by sunlight. The cell was comprised of a custom-made three-electrode setup, with hematite thin film on fluorine-doped tin oxide (FTO) coated glass as working electrode and photoabsorber. A xenon lamp was used to mimic sunlight illumination and the photocurrent density, which is proportional to the water splitting activity,[21] was measured by a potential scan from –1 to +1 V (*vs.* SCE; Fig. 4).

Initial measurements at pH 7 using a homogeneous solution of **2** in water containing 3.5% NaCl as electrolyte revealed an increase of the photocurrent density from 172 to 245 μA cm^2, monitored at 1.23 V *vs* reversible hydrogen electrode (RHE).[22] When considering that the electron transfer between the homogeneously dissolved iridium centers and the hematite photoelectrode is far from ideal, appropriate engineering of the cell is expected to improve this 40% increase substantially. Light is pivotal for inducing catalytic activity, as the corresponding dark current was a mere 8 μA cm^2 at the same potential even in the presence of **2** (Fig. S3).

Variation of the pH had a distinct effect (*cf* Fig. 4). In a basic environment (pH 13.6, adjusted by NaOH), the photoelectrode on its own produced a markedly higher photocurrent. Addition of **2**, however, quenched some of this activity and actually lowered the photoelectrochemical response to about 30%. This detrimental effect may hint to a low stability of **2** under basic conditions, inducing decomposition of inactive material on the photoelectrode. Separate NMR spectroscopic measurements of **2** in aq. NaOH (1 M) revealed a high stability and no traces of complex degradation were detected. Even though instability of complex **2** cannot be discarded completely, such degradation processes would not be expected to lower the activity of the photoelectrode. It is thus more likely that oxidized forms of **2** or **3**, generated as intermediates in the water oxidation cycle, are

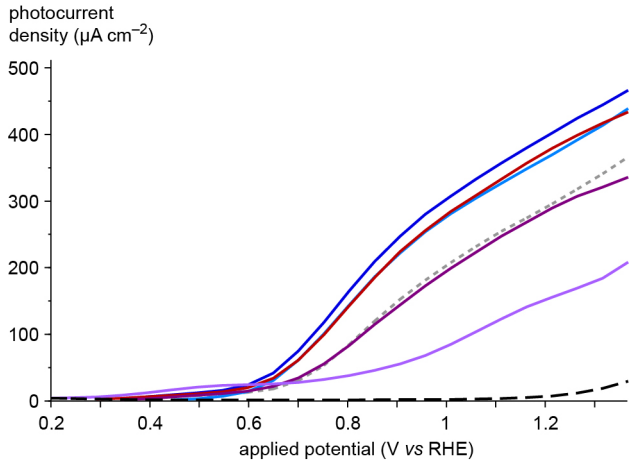

Fig. 5 Effect of different concentrations of complex **2** (0 = dotted grey, dark black dashed, 5.4 μM bright blue, 13 μM dark blue, 27 μM red, 51 μM purple, 140 μM mauve) on the photocurrent of the hematite photoelectrode.

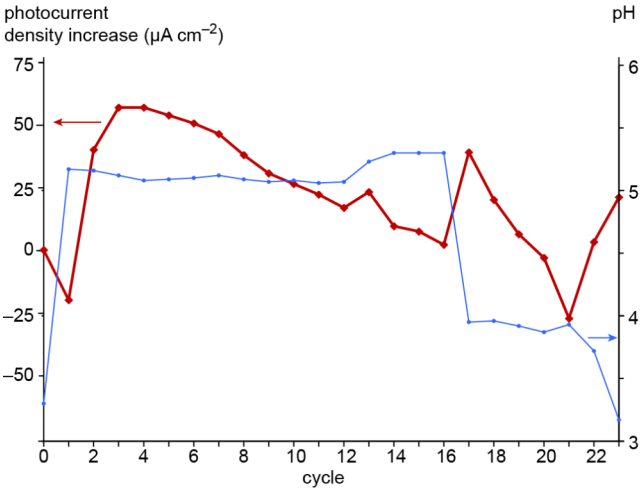

Fig. 6 Photocurrent density generated over multiple photoelectrochemical cycles, and concomitant change of pH. After cycles 16, 21, and 22, HCl was added to re-adjust the pH, leading to an immediate increase in photocurrent response.

more susceptible towards deprotonation and base-induced decomposition than the parent iridium(III) species.

A low pH (3.3, adjusted by H_2SO_4) increased the activity of both the photoelectrode and complex **2**, providing a photocurrent density around 400 μA cm^2 (*cf* 11.2 μA cm^2 in the dark with **2** and hematite). The light-induced activity was highest when the concentration of **2** was in the 5–30 μM range (Fig. 5). The best performance at pH 3.3 was obtained with a 13 μM concentration of **2**, which generated a 33% increase of the photocurrent density as compared to the activity of the bare photoelectrode. Catalyst concentrations of 100 μM and beyond had a detrimental effect and actually lowered the activity of the photoelectrode. Possibly, complexes or more presumably catalytic intermediates are deposited on the electrode during water splitting.[23]

Based on the long-term stability of the catalytically active species in CAN-mediated water oxidation, repetitive photoelectrochemical measurements were carried out with complex **2** under acidic conditions. When using HCl instead of H_2SO_4 for pH adjustment, the increase of the photocurrent density with respect to the non-catalyzed hematite was lower (15±5% rather than 25±5%), though ambiguities with regards to the source of oxygen are reduced. A first scan resulted in a lower photocurrent, but in subsequent cycles, the photocurrent was considerably higher in the presence of complex **2** (Fig. 6). The first scan likely involves a catalyst activation, which is also reflected by the substantial increase of the pH. Subsequent cycles do not modify the pH and thus support a catalyst activation rather than a catalytic process that induces the initial pH leveling. In these subsequent cycles, the iridium-induced photocurrent gradually decreased, unless the pH is influenced. A strong influence of the pH on the catalytic activity is demonstrated by the immediate increase of the photocurrent density upon addition of HCl after cycles 16, 21, and 22.[24] Deactivation rather than degradation of the catalytically active species is further supported by the high turnover numbers that were observed with complex **2** (vide supra). As a plausible rationale for the strongly pH dependent behavior of the photoelectrochemical cell, intermediates of the iridium-catalyzed water oxidation cycle may be electro-deposited on the photoelectrode during scans, thus impeding the electron transfer from dissolved iridium species to the photoabsorber. According to this model, variation of the pH will affect the stability of the electro-deposited species and results in dissociation of these intermediate species, thus restoring the activity of the photoelectrode and the iridium species. For technical applications, such deactivation issues may be resolved by pH oscillation rather than by a continuous increase of the acidity as illustrated in Fig. 6. While extensive testing is still pending, these multiple cycle experiments confirmed that the catalytic activity is lowered, yet not lost. This conclusion is in agreement with the longevity observed for complex **2** and related Ir(Cp*) complexes containing a triazolylidene ligand.[10b]

The enhanced photocurrent produced with complex **2** when using 3.5% NaCl as supporting electrolyte suggested that sea water rather than purified fresh water may be utilizable in the photoelectrochemical cell. Measurements using authentic samples of crudely filtered samples from the Irish Sea were impeded by an unstable photocurrent when using the photoelectrode solely, *i.e.* without addition of complex **2**. Apparently, contaminations in sea water are incompatible with the hematite-functionalized electrode. Parallel work investigated the CAN-mediated oxidation of sea water with complex **2**. While O_2 evolution was qualitative not substantially different in sea water and in pure H_2O, formation of hypochlorite as a product of Cl^- oxidation was noted. Hypochlorite production may also rationalize the lower photocurrent increase when HCl was used rather than H_2SO_4. Even though complex **2** seems to provide a robust catalytically active species that is compatible with sea water, the highly oxidizing microscopic environment at iridium combined with the large chloride concentration of the solute appears to intrinsically prevent a direct use of sea water for water splitting.

Conclusions

An iridium complex derived from an easily accessible triazolylidene ligand displays high potential as water oxidation catalyst. In CAN-mediated oxidation, high turnover numbers are achieved, even though catalytic performance gradually ceases over extended periods of time (several days). The complex is also

active in a photoelectrochemical cell and enhances the photocurrent density. Depositon of intermediate species on the photoelectrode has been observed, which is in parts resolved by modification of the pH of the solution. These studies identified a number of critical factors which may provide guidelines for further engineering of photo(electro)chemical cells: (i) chelation is beneficial, both for the activity and the longevity of the catalytically active water-oxidizing species; (ii) chlorides are prone to be oxidized, thus absorbing some oxygen and reducing the amount of O_2 produced, though neither chloride nor its oxidized congeners are poisoning the catalytic activity of the iridium complex; (iii) hematite photoelectrodes may be more sensitive, when sea water is used; (iv) the electron transfer from the iridium center to the hematite is poor in the current set-up. Physi- or chemisorption of the complex on the photoelectrode may improve the electron transfer and thus the photocatalytic performance substantially. Current work is ongoing to verify these conclusions and to further improve the catalytic cell.

Experimental procedures

General

All syntheses were carried out under an inert atmosphere of N_2 using Schlenk techniques and dry solvents. The 1,3-dimethyl-4-(phenyl)triazolium iodide **1** was synthesized according to literature procedures,[25] all other reagents were commercially available and used as received. All ^{1}H and ^{13}C{^{1}H} NMR spectra were recorded at room temperature on Varian spectrometers and chemical shift were referenced to $SiMe_4$ (δ in ppm, J in Hz). Assignments are based on homo- and heteronuclear shift correlation spectroscopy. Elemental analyses were performed by the Microanalytical Laboratory at University College Dublin, Ireland, using a Exter Analytical CE-440 Elemental Analyzer.

Synthesis of 2

A suspension of 1,3-dimethyl-4-(phenyl)triazolium iodide (200 mg, 0.67 mmol), Ag_2O (155 mg, 0.67 mmol) and $[Cp^*IrCl_2]_2$ (266 mg, 0.34 mmol) in CH_2Cl_2 (20 mL) was stirred under N_2 for 14 h. The resulting mixture was filtered trough Celite and the filtrate was concentrated under vacuum and layered with MeOH (1:1 ratio). Orange crystals of **2** formed upon slow evaporation and were isolated and dried. Yield: 274 mg (73%). ^{1}H NMR (400 MHz, $CDCl_3$, 30 °C): δ 7.68 (m, 2H, H_{Ph}), 7.44 (m, 3H, H_{Ph}), 4.44, 3.73 (2 × s, 3H, N–CH_3) 1.43 (s, 15H, C_{Cp}–CH_3). ^{13}C{^{1}H} NMR (100 MHz, $CDCl_3$, 30 °C): δ 149.4 (C_{trz}–Ph), 144.9 (C_{trz}–Ir), 132.5, 129.8, 127.8 (3 × C_{Ph}–H), 127.6 (C_{Ph}–C_{trz}), 87.9 (C_{Cp}), 41.7, 36.8 (2 × N–CH_3), 8.9 (C_{Cp}–CH_3). Elem Anal calcd for $C_{20}H_{26}Cl_2IrN_3$ (571.56): C 42.03, H 4.59, N 7.35; found: C 41.78, H, 4.36, N, 6.71.

Synthesis of 3

Complex **2** (46 mg, 80 μmol) and sodium acetate (13 mg, 0.16 mmol) were stirred in $ClCH_2CH_2Cl$ (4 mL) under N_2 for 12 h at 60 °C. The resulting mixture was filtered through celite and the solvent removed under vacuum, yielding **3** as a yellow solid (40 mg, 93%). ^{1}H NMR (500 MHz, $CDCl_3$, 30 °C): δ 7.87 (dd, 1H, $^3J_{HH}$ = 7.3 Hz, $^4J_{HH}$ = 1.3 Hz, H_{Ar}), 7.33 (dd, 1H, $^3J_{HH}$ = 7.3 Hz, $^4J_{HH}$ = 1.3 Hz, H_{Ar}), 7.02 (td, 1H, $^3J_{HH}$ = 7.3 Hz, $^4J_{HH}$ = 1.3 Hz, H_{Ar}), 6.96 (td, 1H, $^3J_{HH}$ = 7.3 Hz, $^4J_{HH}$ = 1.3 Hz, H_{Ar}), 4.23, 4.21 (2 × s, 3H, N–CH_3) 1.78 (s, 15H, C_{Cp}–CH_3). ^{13}C{^{1}H} NMR (125 MHz, $CDCl_3$, 30 °C): δ 158.9 (C_{Ar}–Ir), 157.2 (C_{trz}–Ar), 154.0 (C_{trz}–Ir) 137.8 (C_{Ar}–H), 136.4 (C_{Ar}–C_{trz}), 128.7, 121.6, 120.3 (3 × C_{Ar}–H), 89.8 (C_{Cp}), 38.2, 36.2 (2 × N–CH_3), 9.8 (C_{Cp}–CH_3). Elem Anal calcd for $C_{20}H_{25}IrN_3Cl$ (535.14): C 44.89, H 4.71, N 7.85; found: C, 45.13; H, 4.82; N, 7.56.

Photoelectrode preparation

Fluorine-doped tin oxide (FTO) coated glasses were utilized as the substrates for the hematite coating deposition. The substrates were ultrasonically cleaned in acetone followed by methanol, each for 5 min prior to coating deposition and then dried using compressed air to prevent water stains on the surface. The deposition study was performed using a solution-based technique called chemical bath deposition (CBD).[16b,c] The substrate was immersed in an aqueous solution of $FeCl_3.6H_2O$ (0.15 M) and $NaNO_3$ (1 M) at 95 °C for 2 h, with the conductive layer facing outwards. The pH of the solution was adjusted to 1.5 using HCl solution with constant stirring. The FTO glasses were removed after 2 h and washed with distilled water and dried. The films prepared are yellowish and well adherent to the substrates. The dried coated samples were then thermally treated in air in a box furnace at 800 °C for 20 min with heating and cooling rates of 20 °C min^{-1} and 50 °C min^{-1}, respectively.

Photoelectrochemical measurements

The photocurrent density was measured with a custom-made Gamry G300 potentiostat and a Newport 450W solar simulator as photoelectrochemical cell (PEC). The PEC was comprised of hematite thin film as working electrode, a platinum wire (counter electrode), and a saturated calomel electrode (SCE) as reference electrode immersed in solution. The solution (160 mL) was pH-adjusted by NaOH, H_2SO_4, or HCl, and NaCl (3.5 wt%) was added to neutral or acidic solutions. An aqueous solution of complex **2** (0.87 mM) was added (see Fig. 5). Scans were performed at 50 mV s^{-1} between –1.0 and +1.0 V vs SCE, both in the presence and absence of complex **2** and with or without illumination. Simulated sunlight (AM 1.5) from a filtered 450 W xenon lamp was supplied through a fused quartz glass window onto the front side of the photoelectrode surface at a measured intensity of 870 W m^{-2}. The area of light illumination was 0.95 cm^2 and was defined by the plastic holder used to mount the working electrode. All potentials are corrected for starting pH of the electrolyte and reported against the reversible hydrogen electrode (RHE). A pH meter (OMRON E5C2, EUTECH INSTRUMENTS pH 200 Series) was used to constantly monitor the pH of the solution during measurements.

Crystallographic details

Crystal data were collected using an Oxford Diffraction SuperNova A diffractometer fitted with an Atlas detector (Mo–Kα radiation, 0.71073 Å). At five-fold redundant dataset was collected, assuming that the Friedel pairs are not equivalent. An analytical absorption correction based on the shape of the crystal was performed.[26] The structure was solved by direct methods using the program SHELXS-97 and refined by full matrix least squares on F^2 with SHELXL-97.[27] The hydrogen atoms were included in calculated positions and treated as riding atoms using SHELXL-97 default parameters. All non-hydrogen atoms were

refined anisotropically. Further details on data collection and refinement are summarised in Table S1. Crystallographic data (excluding structure factors) have been deposited with the Cambridge Crystallographic Centre as supplementary publication no. CCDC 867256. Copies of the data can be obtained free of charge on application to CCDC, 12 Union Road, Cambridge CB2 1EZ, UK [fax: +44-1223-336-033; e-mail: deposit@ccdc.cam.ac.uk].

Acknowledgements

We thank Science Foundation Ireland, in parts under the Solar Energy Conversion Strategic Research Cluster, for funding (SFI grants No. 07/SRC/B1160 and CHS2844). We gratefully acknowledge support by the European Research Council (ERC-StG 208651 to M.A.) and by the National Science Foundation (CHE-1055547 to S.B.).

Notes and references

[a] *School of Chemistry & Chemical Biology, University College Dublin, Belfield, Dublin 4, Ireland. Fax: +353 1716 2501; Tel: +353 1716 2504; E-mail: martin.albrecht@ucd.ie*

[b] *SFI Strategic Research Cluster in Solar Energy Conversion.*

[c] *School of Chemical & Bioprocess Engineering, University College Dublin, Belfield, Dublin 4, Ireland.*

[d] *Department of Chemistry, Carnegie Mellon University, Pittsburgh, Pennsylvania 15213, United States.*

† Electronic Supplementary Information (ESI) available: Stacked plot of UV vis spectra of **2** and inverse absorption plots at different Ce^{IV} concentrations, comparison of dark and photocurrent with **2**, crystallographic details. See DOI: 10.1039/b000000x/

1 *a*) Energy Information Administration (2011) *International Energy Outlook* (US Dept of Energy, Washington, DC); *b*) N. D. McDaniel and S. Bernhard, *Dalton Trans.*, 2010, **39**, 10021–10030.

2 *a*) K. N. Ferreira, T. M. Iversion, K. Maghlaoui, J. Barber and S. Iwata, *Science*, 2004, **303**, 1831–1838; *b*) J. P. McEvoy and G. W. Brudvig, *Chem. Rev.*, 2006, **106**, 4455; *c*) Y. Umena, K. Kawakami, J.–R. Shen and N. Kamiya, *Nature*, 2011, **473**, 55–60.

3 *a*) L. Hammarström and S. Hammes-Schiffer, *Acc. Chem. Res.*, 2009, **42**, 1859–1860 (special issue); *b*) M. G. Walter, E. L. Warren, J. R. McKone, S. W. Boettcher, Q. Mi, E. A. Satori and N. S. Lewis, *Chem. Rev.*, 2010, **110**, 6446–6473; *c*) H. Dau, C. Limberg, T. Reier, M. Risch, S. Roggan and P. Strasser, *ChemCatChem*, 2010, **2**, 724–761; *d*) C. Herrero, A. Quaranta, W. Leibl, A. W. Rutherford and A. Aukauloo, *Energy Environ. Sci.,* 2011, **4**, 2353; *e*) E. S. Andreiadis, M. Chavarot-Kerlidou, M. Fontecave and V. Artero, *Photochem Photobiol.*, 2011, **87**, 946–964; *f*) S. Y. Reece, J. A. Hamel, K. Sung, T. D. Jarvi, A. J. Esswein, J. J. H. Pijpers and D. G. Noceera, *Science*, 2011, **334**, 645–648.

4 R. Eisenberg and H. B. Gray, *Inorg. Chem.,* 2008, **47**, 1697.

5 *a*) S. Romain, L. Vigara and A. llobet, *Acc. Chem. Res.*, 2009, **42**, 1944–1953; *b*) Z. Chen, J. J. Concepcion, X. Hu, W. Yang, P. G. Hoertz, T. J. Meyer, *Proc. Nat. Acad. Sci. USA,* 2010, **107**, 7225; *c*) L. Vilella, P. Vidossich, D. Balcells and A. Lledos, *Dalton Trans.,* 2011, **40**, 11241; *d*) S. Gosh and M.-H. Baik, *Angew. Chem. Int. Ed.*, **2012**, *51*, in press (DOI: 10.1002/anie.201106337).

6 For examples of heterogeneous catalyst precursors and semiconductor approaches, see: *a*) M. W. Kanan and D. G. Nocera, *Science*, 2008, **321**, 107; *b*) W. J. Youngblood, S. H.-A. Lee, K. Maeda and T. E. Mallouk, *Acc. Chem. Res.*, 2009, **42**, 1966; *c*) Y. Surendranath, M. Dinca and D. G. Nocera, *J. Am. Chem. Soc.*, 2009, **131**, 2615; *d*) E. M. P. Steinmiller and K. S. Choi, *Proc. Natl. Acad. Sci. USA*, 2009, **106**, 20633; *e*) M. Dinca, Y. Surendranath and D. G. Nocera, *Proc. Natl. Acad. Sci. USA*, 2010, **107**, 10337; *f*) S. D. Tilley, M. Cornuz, K. Sivula and M. Grätzel, *Angew. Chem. Int. Ed.*, 2010, **49**, 6405; *g*) N. H. Chou, P. N. Ross, A. T. Bell and T. D. Tilley, *ChemSusChem*, 2011, **4**, 1566–1569.

7 For a brief review, see: *a*) X. Sala, I. Romero, M. Rodriguez, L. Escriche and A. Llobet, *Angew. Chem. Int. Ed.* 2009, **48**, 2842; for key examples, see: *b*) S. W. Gersten, G. J. Samuels and T. J. Meyer, *J. Am. Chem. Soc.*, 1982, **104**, 4029; *c*) C. Sens, I. Romero, M. Rodriguez, A. Llobet, T. Parella and J. Benet-Buchholz, *J. Am. Chem. Soc.*, 2004, **126**, 7798; *d*) R. Zong and R. P. Thummel, *J. Am. Chem. Soc.*, 2005, **127**, 12802; *e*) Z. Deng, H. Tseng, R. Zong, D. Wang and R. Thummel, *Inorg. Chem.*, 2008, **47**, 1835; *f*) A. Sartorel, M. Carraro, G. Scorrano, R. De Zorzi, S. Geremia, N. D. McDaniel, S. Bernhard and M. Bonchio, *J. Am. Chem. Soc.*, 2008, **130**, 5006; *g*) Y. V. Geletii, B. Botar, P. Koegerler, D. A. Hillesheim, D. G. Musaev and C. L. Hill, *Angew. Chem. Int. Ed.*, 2008, **47**, 3896; *h*) A. Sartorel, P. Miro, E. Salvadori, S. Romain, M. Carraro, G. Scorrano, M. Di Valentin, A. Llobet, C. Bo and M. Bonchio, *J. Am. Chem. Soc.*, 2009, **131**, 16051; *i*) M. M. Najafpour, T. Ehrenberg, M. Wiechen and P. Kurz, *Angew. Chem. Int. Ed.* 2010, **49**, 2233–2237; *j*) Q. Yin, J. M. Tan, C. Besson, Y. V. Geletii, D. G. Musaev, A. E. Kuznetsov, Z. Luo, K. I. Hardcastle and C. L. Hill, *Science*, 2010, **328**, 342; *k*) N. S. McCool, D. M. Robinson, J. E. Sheats and G. C. Dismukes, *J. Am. Chem. Soc.*, 2011, **133**, 11446.

8 *a*) N. D. McDaniel, F. J. Coughlin, L. L. Tinker and S. Bernhard, *J. Am. Chem. Soc.*, 2008, **130**, 210; *b*) S. W. Kohl, L. Weiner, L. Schwartsburd, L. Konstantinovski, L. J. W. Shimon, Y. Ben-David, M. A. Iron and D. Milstein, *Science*, 2009, **324**, 74; *c*) J. F. Hull, D. Balcells, J. D. Blakemore, C. D. Incarvito, O. Eisenstein, G. W. Brudwig and R. H. Crabtree, *J. Am. Chem. Soc*., 2009, **131**, 8730–8731; *d*) W. C. Ellis, D. McDaniel, S. Bernhard, T. J. Collins, *J. Am. Chem. Soc.* 2010, **132**, 10990; *e*) J. F. Hull, D. Balcells, J. D. Blakemore, C. D. Incarvito, O. Eisenstein, G. W. Brudwig, R. H. Crabtree, *J. Am. Chem. Soc*. 2009, **131**, 8731; *f*) J. L. Fillol, Z. Codola, I. Garcia-Bosch, L. Gomez, J. J. Pla and M. Costas, *Nature Chem*., 2011, **3**, 807; *g*) L. Bernet, R. Lalrempuia, W. Ghattas, H. Mueller-Bunz, L. Vigara, A. Llobet and M. Albrecht, *Chem. Commun*., 2011, **47**, 8058.

9 M. H. V. Huynh and T. J. Meyer, *Chem. Rev.*, 2007, **107**, 5004.

10 *a*) J. D. Blakemore, N. D. Schley, D. Balcells, J. F. Hull, G. W. Olack, C. D. Incarvito, O. Eisenstein, G. W. Brudvig and R. H. Crabtree, *J. Am. Chem. Soc.*, 2010, **132**, 16017; *b*) R. Lalrempuia, N. D. McDaniel, H. Müller-Bunz, S. Bernhard and M. Albrecht, *Angew. Chem. Int. Ed.*, 2010, **49**, 9765; *c*) A. Savini, G. Bellachima, G. Ciancaleoni, C. Zuccaccia, D. Zuccaccia and A. Macchioni *Chem. Commun.*, 2010, **46**, 9218; *d*) J. D. Blakemore, N. D. Schley, G. Olack, C. D. Incarvito, G. W. Brudvig and R. H. Crabtree, *Chem. Sci.*, 2011, 2, 94–98; *e*) D. G. H. Hetterscheid and J. N. H. Reek, *Chem. Commun.,* 2011, **47**, 2712.

11 *a*) N. D. Schley, J. D. Blakemore, N. K. Subbaiyan, C. D. Incarvito, F. D'Souza, R. H. Crabtree and G. W. Brudvig, *J. Am. Chem. Soc.*, 2011, **133**, 10473; *b*) D. B. Grotjahn, *J. Am. Chem. Soc.*, 2011, **133**, 19024; *c*) N. Marquet, F. Gärtner, S. Losse, M.-M. Pohl, H. Junge, M. Beller, *ChemSusChem*, 2011, **4**, 1598–1600; *d*) A. Savini, P. Belanzoni, G. Bellachioma, C. Zuccaccia, D. Zuccaccia, A. Macchioni, *Green Chem.* 2011, **13**, in press (DOI:10.1039/c1gc15899f).

12 R. Lalrempuia, J. A. Woods, A. Petronilho, N. D. McDaniel, H. Müller-Bunz, M. Albrecht and S. Bernhard *in preparation*.

13 a) P. Mathew, A. Neels, M. Albrecht, *J. Am. Chem. Soc.*, 2008, **130**, 13534–13535; *b*) G. Guisado-Barrios, J. Bouffard, B. Donnadieu and G. Bertrand, *Angew. Chem. Int. Ed.* **2010**, *49*, 4759–4762; *c*) O. Schuster, L. Yang, H. G. Raubenheimer and M. Albrecht, *Chem. Rev.*, 2009, **109**, 3445–3478; *d*) J. D. Crowley, A.-L. Lee and K. J. Kilpin, *Aust. J. Chem.*, 2011, **64**, 1118–1132.

14 *a*) A. Krüger and M. Albrecht, *Aust. J. Chem.*, 2011, **64**, 1113; *b*) A. Krüger, L. J. L. Häller, H. Müller-Bunz, O. Serada, A. Neels, S. A. Macgregor and M. Albrecht, *Dalton Trans.*, 2011, **40**, 9911; *c*) A. Krüger and M. Albrecht, *Chem. Eur. J.*, 2012, **18**, 652.

15 *a*) Y. Xu, A. Fischer, L. Duan, L. Tong, E. Gabrielsson, B. Akermark and L. Sun, *Angew. Chem. Int. Ed.*, 2010, **49**, 8934–8937; *b*) G. F. Moore, J. D. Blakemore, R. L. Milot, J. F. Hull, H. Song, L. Cai, C. A. Schmuttenmaer, R. H. Crabtree and G. W. Brudwig, *Energy Environ. Sci.,* 2011, **4**, 2389–2392.

16 *a*) K. Sivula, F. Le Formal and M. Grätzel, *ChemSusChem*, 2011, **4**, 432–449; *b*) L. Vayssieries, N. Beermann, S.-E. Lindquist and A. Hagfeldt, *Chem. Mater*., 2001, **13**, 233-235; *c*) R. Morrish, M. Rahman, J. M. D. MacElroy and C. Wolden, *ChemSusChem*, 2011, **4**, 474-479.

17 For examples, see: *a*) K. J. Kilpin, U. S. D. Paul, A.-L. Lee and J. D. Crowley, *Chem. Commun.*, 2010, **47**, 328; *b*) A. Prades, E. Peris and M. Albrecht, *Organometallics*, 2011, **30**, 1162; *c*) R. Saravanakumar, V. Ramkumar and S. Sankararaman, *Organometallics*, 2011, **30**, 1689; *d*) J. Bouffard, B. K. Keitz, R. Tonner, G. Guisado-Barrios, G. Frenking, R. H. Grubbs and G. Bertrand, *Organometallics*, 2011, **30**, 2617; *e*) J. Cai, X. Yang, K. Arumugam, C. W. Bielawski and J. L. Sessler, *Organometallics*, 2011, **30**, 5033; *f*) T. Nakamura, T. Terashima, K. Ogata and S.-I. Fukuzawa, *Org. Lett.* 2011, **13**, 620; *g*) E. M. Schuster, M. Botoshansky and M. Gandelman, *Dalton Trans.*, 2011, **40**, 8764.

18 For examples, see: *a*) K. Ohmatsu, M. Kiyokawa and T. Ooi, *J. Am. Chem. Soc.*, 2011, **133**, 1307-1309; *b*) Q-H. Liu, Y.-C. Li, Y.-Y. Li, Z. Wang, W. Liu, C. Qi and S.-P. Pang, *J. Mater. Chem.,* 2012, **22**, 666-674; *c*) G. Kaplan, G. Drake, K. Tollison, L. Hall and T. Hawkins, *J. Heterocyclic Chem.*, 2005, **42**, 19-27.

19 A. Poulain, D. Canseco-Gonzalez, R. Hynes-Roche, H. Müller-Bunz, O. Schuster, H. Stoeckli-Evans, A. Neels and M. Albrecht, *Organometallics,* 2011, **30**, 1021

20 Previous work on single-site ruthenium complexes containing a triazolylidene ligand suggested that an N-bound phenyl *ortho* substituent on the heterocycle is deterioriating O_2 production and affords detectable quantities of CO_2 (see ref. 8*g*). The constantly high activity of **2** over tens of hours suggests that such degradation is neglegible here, indicating a fundamentally different impact of *C*- vs *N*-positioned phenyl groups.

21 M. Rahman, B. H. Q. Dang, K. McDonnell, J. M. D. MacElroy and D. P. Dowling, *J. Nanosci. Nanotechnol.*, 2012, in press (doi:10.1166/jnn.2012.4897).

22 A. Kay, I. Cesar and M. Grätzel, *J. Am. Chem. Soc.*, 2006, **128**, 15714-15721.

23 Alternatively, reactions may take place in a sequential manner at the electrode, and hence diffusion is not limiting.

24 An increase of catalytic activity was also observed upon raising the pH, demonstrated by the enhanced activity in cycle 12 after an undeliberate increase of the pH of the solution.

25 D. Canseco-Gonzalez, A. Gniewek, M. Szulmanowicz, H. Müller-Bunz, A. Trzeciak and M. Albrecht, *Chem. Eur. J.*, 2012, **18**, in press.

26 Program CrysalisPro Version 1.171.33.55, Oxford Diffraction Limited, 2010. Analytical numeric absorption correction using a multifaceted crystal model were based on expressions derived by Clark and Reid: R. C. Clark and J. S. Reid, *Acta Cryst.,* 1995, **A51**, 887.

27 G. M. Sheldrick, *Acta Cryst.,* 2008, **A64**, 112.